THE PENNSYLVANIA STATE UNIVERSITY
SCHREYER HONORS COLLEGE

DEPARTMENT OF NUCLEAR ENGINEERING

Feasibility of High-Frequency Radiation for Electrical Energy Generation in Fusion Devices

COLEMAN SMITH
SPRING 2023

A thesis
submitted in partial fulfillment
of the requirements
for baccalaureate degrees
in Nuclear Engineering
with honors in Area of Nuclear Engineering

Reviewed and approved* by the following:

Martin de Jesus Nieto-Perez
Associate Teaching Professor
Thesis Supervisor

Elia Merzari
Associate Professor of Nuclear Engineering
Honors Adviser

*Electronic approvals are on file.

Abstract

In modern approaches to practical nuclear fusion power, the primary means of energy generation is assumed to be thermal energy extracted from the products of the fusion reaction. While this indeed makes up a vast majority of the energy yield from fusion reactions, there are of course several other forms through which this energy yield is dissipated, resulting in energy losses, and bringing the necessary Q value, that is, the fusion energy out versus that which is invested into driving the reaction, for economic energy extraction higher. In order to better understand the physics that occurs in these devices, it is necessary to develop diagnostics that can give the greatest level of detail about the system. In this project, a means of direct conversion of ionizing radiation energy from fusion to electrical energy is proposed from the results of rigorous calculation. This new mechanism would provide a means of analyzing the soft x-ray spectrum produced during operation of a fusion device that uses minimal volume in the design of a tokamak or stellarator. Using single crystals of methylammonium lead iodide, which has shown promising results in laboratory settings to generate photo-currents from x-ray bombardment, a hypothetical energy yield will be calculated from computation. Models generated in OpenMC and IMD showed potential for the material to be used in radiation detection technology for fusion devices, but not as a form of energy recapture.

Table of Contents

List of Figures

List of Tables

Acknowledgements

I would like to acknowledge Dr. Martin Nieto-Perez, Dr. Elia Merzari, and Dr. Jean Paul Allain for enabling me to explore this fascinating topic within nuclear engineering, while also guiding me throughout my journey in nuclear engineering at the Schreyer Honors College. I would also like to thank the members of the IGNIS-2 Lab and the Nanofabrication Lab for allowing me to work with their lab spaces to conduct this research.

Chapter 1

Introduction

1.1 Background on Diagnostics in Fusion Devices and Project Motivation

In a system dominated by the stochastic properties of fluid motion and the infinitesimal speeds of nuclear interactions, there is little wonder why diagnostic devices are vital to the successful operation of a fusion reactor. A visual testament to the complexity of such technology can be seen in a very detailed physics simulation render found in Figure 1.1.

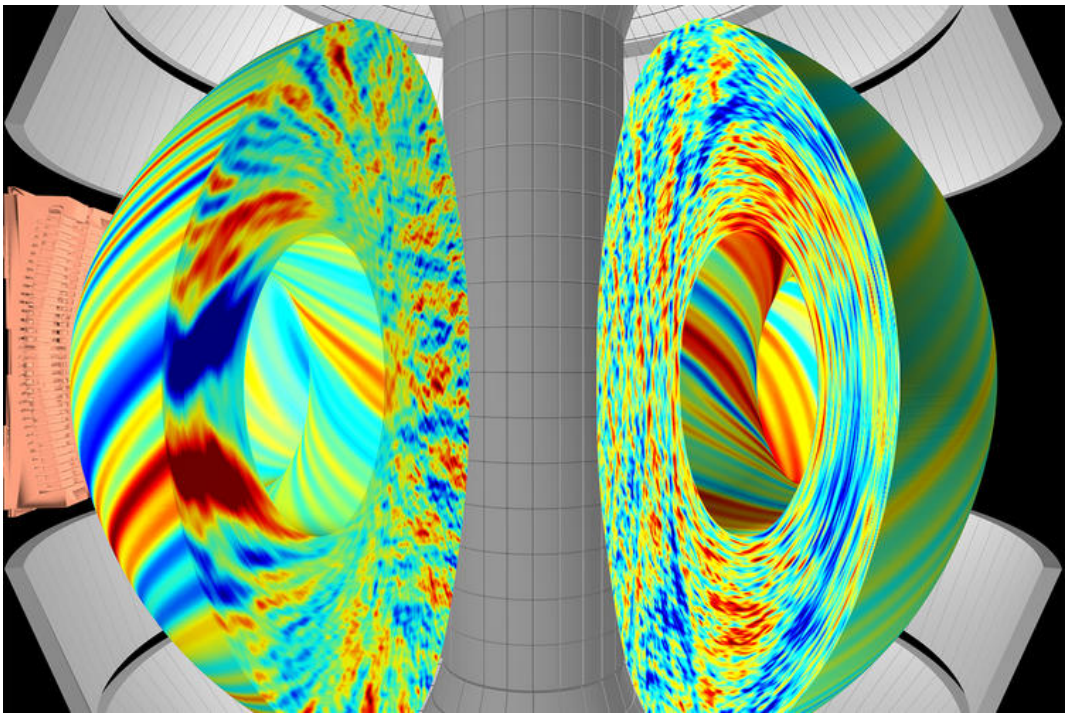

Figure 1.1: A render of PPPL's NSTX-U tokamak [1]

Plasma scientists and engineers are particularly interested in tracking the evolution of the heat, magnetic field, charge movement, and radiation generation in fusion devices [2]. These parameters are of interest because they help paint a very clear picture of what to expect as time progresses during operation. As these diagnostic devices improve, so will our ability to control plasmas. This is why it is imperative to the advancement of the field that novel means of tracking these parameters within fusion devices become more sophisticated with time. For the scope of this project, potential for a radiation detector diagnostic will be of primary focus. The goal of this project will be to determine if a given candidate material is usable for a new set of radiation detection diagnostics in fusion devices, and to propose a means of validating calculations and predictions made from this project.

1.2 Analyzing Fusion Device Transients from Soft X-ray Radiation

The interactions between charged particles within fusion reactors have low energy relative to other devices such as accelerators or fission-based nuclear reactors. This causes the electromagnetic radiation released from fusion interactions, typically through bremsstrahlung, line, cyclotron, or synchrotron radiation, to also be much lower than what is considered typical of accelerators or fission reactors. In fact, these radiation photon energies tend to be on the order of just 1-10 keV, which places these photon energies just on the outskirts of the x-ray regime on the E-M spectrum. The reason that low energy, soft x-rays are common within terrestrial plasma processes is first due to the low centers of mass on the fuel particles involved, which are typically charged isotopes of low atomic number such as hydrogen, helium, or lithium [3, 4]. Another reason why emitted radiation from fusion devices tends to be in the low-energy x-ray spectrum is that this type of radiation is bounded by the kinetic energy of the electrons in the system [4]. It follows from the conservation of energy that the maximum energy of a photon emitted by the deceleration of an electron about a positively charged ion cannot exceed its total kinetic energy. For a plasma with a 5 keV electron temperature, a typical value for most modern fusion devices [4], the maximum energy of photons emitted from electron and ion interactions within this particular plasma is going to be approximately 5 keV. However, this energy is rarely dissipated in a single interaction. The modal photon energy emitted from such plasmas typically a fraction of the plasma temperature itself.

Such properties of the nuclear interactions in a fusion device make them useful for analyzing transients like plasma discharges [2]. By having many soft x-ray detectors placed throughout a hypothetical reactor chamber, individuals seeking to track how the system evolves with respect to the geometry of the chamber would now have a new method of doing so reliably. Being able to see such radiation throughout the chamber would also help analyze disruptive patterns in plasma behavior like magnetic island formation events due to their likelihood of emitting distinct radiation just beyond this energy range as well [5]. Thus, it follows that an excellent novel form of radiation detection within fusion devices would be one that can, with very little space inside the device itself, accurately measure the soft x-rays in real time as a fusion device operates.

Chapter 2

Proposed Experimental Setup

2.1 A Description of an Experiment to Test Photocurrent Production in Methylammonium Lead Iodide Crystals

After establishing the goals of this project, an experiment for validating the possibility of using Methylammonium Lead Iodide Crystals was established. The set of real-world validation experiments were then planned to be conducted at the IGNIS-2 facility at the RSSEL Lab to compliment computational results and expand on the predictions made. The IGNIS-2 facility is a materials analysis station comprised of several pieces of material surface testing equipment. The device of particular interest for the proposed set of experiments is the RMC50 x-ray source fixed to the system's primary vacuum chamber. This source can be used to generate x-rays in an energy range comparable to that of bremsstrahlung, line, or synchrotron x-ray radiation found in fusion devices like reactors or related plasma experiments.

Using this form of x-ray generation, a sample of a highly promising material for this process, methylammonium lead iodide ($CH_3NH_3PbI_3$), is proposed to be irradiated in the vacuum chamber at high vacuum conditions while placed in parallel with a picoammeter to track photoelectric events that arise from x-ray source exposure. After synthesising and extracting the methylammonium lead iodide crystal film, a real film could then be fitted with appropriate electronic contacts and tested in a such a high vacuum with the monochromatic x-ray source's interchangeable aluminum and silver-aluminum combined anodes. Shown in Figure 2.1 is a parameterized image of the x-ray source used at the IGNIS-2 facility.

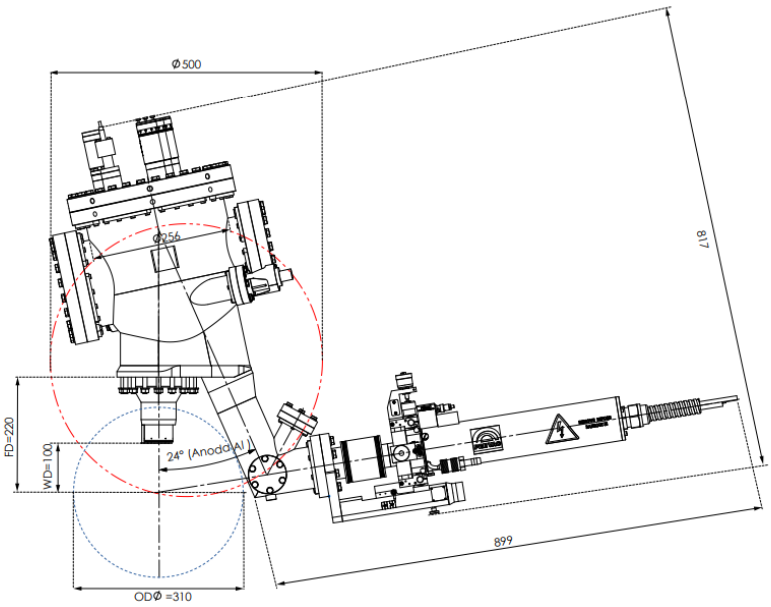

Figure 2.1: RMC50 x-ray source with side profile dimensions [6]

The x-rays produced by both the aluminum and silver anodes are in the single keV range, which is the ideal for recreating the x-ray emissions from both bremsstrahlung and line radiation in a modern fusion device. Several trials can be run at varying photon stream trajectories for each anode. The purpose of varying the trajectory of the beam across multiple trials is multi-functional.

By collecting and comparing data at different x-ray flux trajectories on the same sample, this allows for a precise determination of the focal point of the beam while also verifying the sample's resilience against multiple consecutive irradiation trials. The resultant data may then be interpreted and evaluated for trends in photocurrent production from these photon fluxes.

2.2 Experimental Setup: Preparation of the Methylammonium Lead Iodide Samples

To begin trials for experimentation, a film of methylammonium lead iodide first needed to be synthesized in a laboratory setting. Initially, the proposed synthesis technique involved the creation of a crystal using a precipitation reaction. The overall chemical reaction for the first method first considered can be seen in Equation 2.1:

$$CH_3NH_2(aq) + Pb\left(C_2H_3O_2\right)_2(aq) + 3HI(aq) \rightarrow CH_3NH_3PbI_3(aq) + H_2O(l) + 2C_2H_3O_2^-(aq) \tag{2.1}$$

This method was deferred, however, due to the temporal and logistical constraints it imposed. Other experimenters working with the material saw successful, and much more convenient methylammonium lead iodide synthesis using what is commonly referred to as a "spin coating" technique. This method involves taking small amounts of concentrated reagents for the same crystal synthesis, and spinning them at rotational speeds of over 1000 rpm across a given temperature gradient, which enables rapid growth of thin crystal films on the order of seconds to minutes depending on conditions and desired film thickness. This method also allows for rapid development of a uniform coating of the target crystal on a substrate as opposed to a very slow, imprecise growth of the crystal from precipitation [7, 8, 9]. The chemical pathway for this synthesis, outlined in Equation 2.2, also simplifies the process by requiring just two much more easily-sourced reagents.

$$CH_3NH_2I(aq) + PbI(s) \rightarrow CH_3NH_3PbI_3(s) \tag{2.2}$$

This method, for an experimenter at the Pennsylvania State University, can be performed at the Nanofabrication Laboratory. From the spin coating process, a crystal film of up to 1 micrometer length may easily be produced in just a few minutes [7, 8]. To make electrical sign collection portion of the proposed experiment more convenient, the crystal can be grown on an what is commonly known as an ITO-coated glass substrate. This material, which is widely used throughout the photovoltaics industry, gives the advantage of being both invisible to most photon energies beyond the infrared range while also establishing a thin conductor between the crystal and the glass itself. This conductor is the ITO coating itself, which stands for Indium Tin Oxide and is typically coated in thin layers of just a few hundred angstroms on a float glass substrate [10].

2.3 Experimental Setup: Irradiation of the Methylammonium Lead Iodide Samples

After being synthesized, the crystal film can then be prepared for irradiation by the x-ray source. To measure the generated photocurrent, a conductor would be soldered onto the exposed

surface of the methylammonium lead iodide. This conductor would need to be drawn into a very thin wire to avoid covering the surface of the methylammonium lead iodide as much as possible. It would also need to have a very low internal resistance to prevent further losses to the already small photocurrent this film would produce. For these reasons, the ideal candidate for the conductor would likely be gold. The anode and cathode leads from the film setup would then be connected in series to a picoammeter to then measure the induced photocurrent. Shown in Figure 2.2 is a simple idealized block diagram of the final assembly which would be irradiated by the RMC50 device

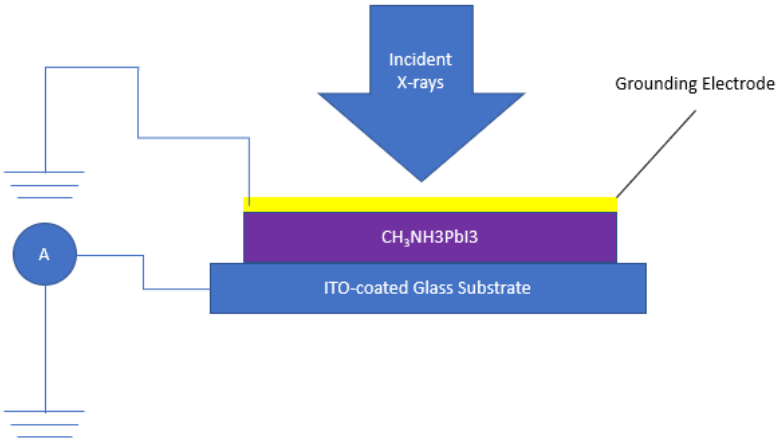

Figure 2.2: A block diagram of the experimental apparatus to be tested with the RMC50 x-ray source

Once a high vacuum is established, the film would be inserted into the vacuum chamber at the IGNIS-2 facility. The source will then used to irradiate the sample. The sample will then be run in 60-second intervals at different angles for each available x-ray source anode. The induced photocurrent would be monitored and recorded by a picoammeter, assuming the sample is capable of producing a photocurrent of at least 1 picoampere. Results of these runs can then be used to verify the true trajectory of the x-ray source beam, and to make predictions about how the material may behave at different photon energies that are also relevant to the operation of fusion devices.

Chapter 3

Computational Approaches

3.1 Computational Modeling Software Choices

Two major packages of software were used in a preliminary analysis of the experimental setup. To get an initial set of predictions for outcomes of this experiment, and to screen for any major shortcomings in the planned experiment, the experimental setup was modeled in a Monte-Carlo simulation and an optical function calculator. The optical function calculator was used to get an idea of how incident light reacts with the sample across multiple ranges of parameters. The Monte-Carlo calculations were also used to make predictions about the sample's interaction with photons, in addition to predictions of how much energy, and through what mechanisms the energy of the absorbed photons was generated.

The first software choice based on the experimental setup was Reflective X-ray Optics LLC's IMD. IMD is a physics modeling software specifically designed for interactions between x-ray photons and a variety of optically-thin films of target material [11]. This software will be primarily used to make initial predictions of the individual optical interactions of the photon flux in the samples along with a prediction of possible leakage through the film. Though this software is ideally written for use in modelling "thin" films-that is, films whose thicknesses are on the magnitude of nanometers-it will be used in this study on a comparatively "thick", one micrometer thickness film. This was not of concern for this project as the theory used to calculate the optical functions for multilayer films in this theory holds for any thickness [11]

A simulation of the experimental setup was also run in MCNP6.20, a neutral particle code well-known by the nuclear science and technology community. A fixed-source trial will be run in MCNP6.20, first considering only an x-ray from the aluminum anode, then the silver anode of the lab x-ray source. Results from the pure x-ray irradiation cases from both software will be compared to determine a range of possible outcomes of the real-world experimental component.

3.2 Modeling Crystal Irradiation in MCNP6.20

To characterize the impact of irradiating the methylammonium lead iodide in all radiation fields of interest for this project, two sets of MCNP input decks were developed. One set simulated the radiation produced from the x-ray source using its aluminum anode. The other was run with a radiation field whose photon energies were comparable to those produced from the silver anode.

The first task of this simulation was to determine an appropriate geometry of the crystal film for irradiation. Compared to the rest of the model, this was quite simple. The crystal was entered into the run deck as a 1 micrometer by 20 millimeter by 20 millimeter rectangular prism with a density comparable to those found in other experimental studies of the material [12]. The areal dimensions were chosen based on real-world experimental results such that the crystal area was conservatively small, but not so small that the film could potentially be dwarfed by the size of the x-ray source spot. Methylammonium lead iodide can be formed at thicknesses thinner than a single micrometer through spin-coating techniques so this model reflects real-world manufacturing techniques. These crystals also grow slowly, on the order of micrometers per minute at rotational speeds of over 5000 rpm, so the small mass sets a realistic basis for the actual crystal size and dimensions [8]. For use in MCNP, the sample generated for irradiation would be considered unusually thin for a photon radiation shielding problem. However, in prior studies, methylammonium lead iodide was shown to have nearly 100% absorption of a uniform, incident photon flux with photon energies of up to

0.1 MeV, or 100 keV, at a duration of up to approximately 30 seconds continuously [9]. Therefore, because the x-ray energies of interest for this problem are considerable lower in energy, having this low of a thickness for the sample was not of concern for the low-energy x-ray radiation either. Identically to the IMD input, a layer of ITO coating and silicon dioxide was placed tangentially behind the methylammonium lead iodide film to simulate the substrate on which the film would be prepared.

With the materials and geometries modeled, the next task was to model the radiation sources themselves. Modeling began with the energies from the monochromator of the lab-based x-ray source. The real-world lab source to be used was a PREVAC Precision Vacuum and Technology RMC50 Monochromatic X-ray Source. Since the real-world compliment uses up to two anodes with a monochromator, it was first decided that the all x-ray sources in these cases would be monochromatic as the real-world source would be nearly monochromatic itself. This set was comprised of two cases, in which an x-ray source corresponding to the photon energies of each of the two electrodes was modeled. The first case, corresponding to the aluminum anode, had the source photon energy set to 1.4866 keV. The second case, corresponding to the silver anode, had the source photon energy set to 2.9843 keV. These values were provided by the manufacturer, along with a value for a possible magnesium anode, which is not currently available for use in this device at the IGNIS-2 Lab at the time of writing this thesis. These values are laid out with their corresponding photon wavelengths in Table 3.1.

Anode material	**Energy [eV]**	**Wavelength [Å]**
Mg	1253.6	9.89
Al	1486.6	8.34
Ag	2984.3	4.155

Table 3.1: List of provided RMC50 anodes detailing their corresponding photon energies and wavelengths [6]

Since energy deposition in the target film is the value of primary interest, it was decided to use a homogeneous planar source for each photon energy with only void in front of the film. MCNP has the ability to track the physics of many aspects of the input. For this project, the parameters of interest to track are the total energy deposition in the film, average energy deposition in the film, other interactions between the photons and the entire sample itself, and the anticipated amount of scattering throughout the duration of the simulation. MCNP tracks many of these parameters by default. However, to track energy deposition, the F6 tally was used in each case. Samples of the MCNP input decks used are available in Appendices A and B.

3.3 Modeling Crystal Irradiation in IMD

To characterize and make predictions on the optical behavior of the irradiation of the methylammonium lead iodide film by an x-ray source, IMD was then used to develop an set of calculations for the lab x-ray sources. From the functions built into this software, the anticipated absorption, reflection, and scattering in the methylammonium lead iodide chip was determined.

Modeling of the film in IMD began with inserting a one micrometer-thick layer of the methylammonium lead iodide sample of interest. Shown in Figure 3.1 is an image of the creation of the methylammonium sample material in IMD's configuration user interface.

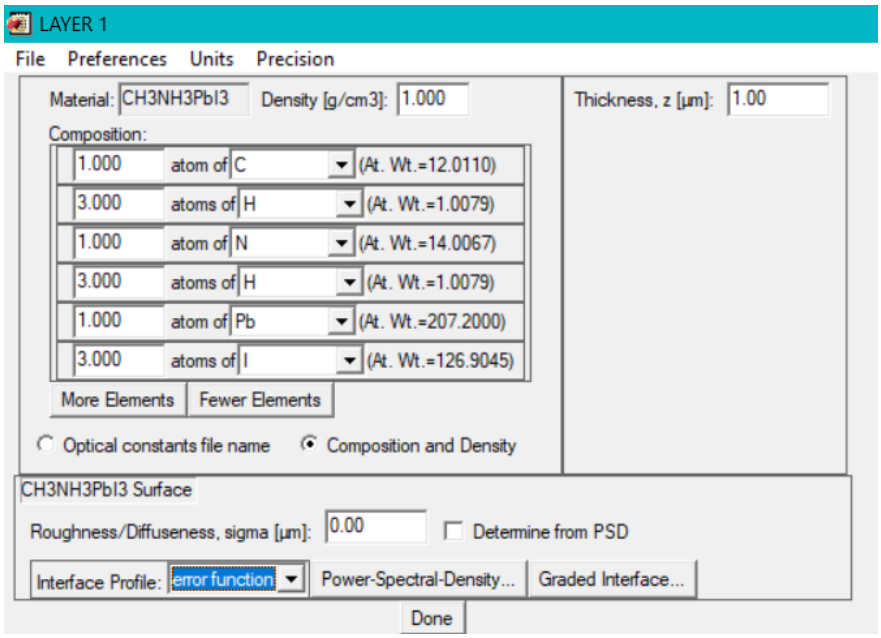

Figure 3.1: IMD material creation interface showing the user-defined creation of methylammonium lead iodide

A substrate was added beneath this layer since the real-world trial will need a substrate to make the film transportable for loading into a sample holder. A convenient access point for measuring induced photocurrent and photo-voltage will also be necessary. This is another requirement for the substrate in the model. To meet both of these requirements, TSO-coated glass was chosen as a substrate. This was modeled as a 0.19 micrometer thickness layer of TSO, which chemically is recognized as $Sn : In_2O_3$ and a layer of simple float glass, assumed to be a homogeneous sample of SiO_2. IMD does not take thickness of a material designated as a substrate into account as it assumes that only the optical properties of the sample itself are of interest. The densities used in this computation were computed using the same method as mentioned in Section 3.2. The prepared sample for simulation can be seen in the overview screen of IMD in Figure 3.2.

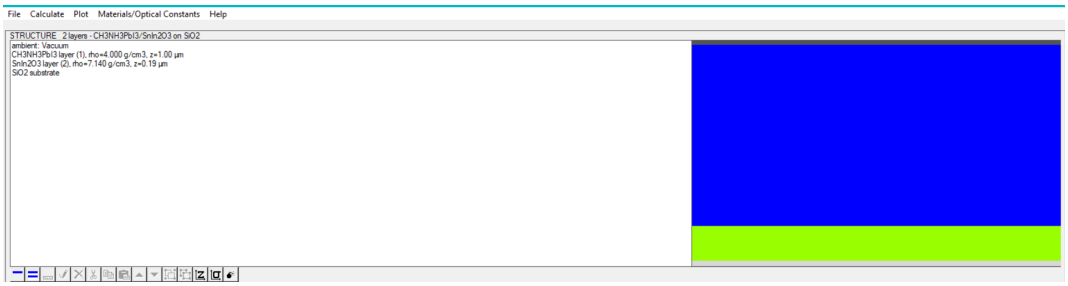

Figure 3.2: IMD main screen with cross-sectional sample display

3.4 Photocurrent Production Considerations for the Surface of a Methylammonium Lead Iodide Film

Since the beam produced from the x-ray device will have to be aimed with varying spatial coordinates normal to the methylammonium lead iodide film and the beam's cross section, a preliminary calculation of response curve of the anticipated photocurrent produced versus the fraction of the beam's cross-sectional area hitting the film was also performed. While the sample can be easily brought near where the x-ray beam spot will likely be, it is highly unlikely that the film will be perfectly centered on the film without any precise measurement. It is however highly possible that the initial positioning of both the beam and the sample is such that the two do not make contact as depicted in Figure 3.3. This would cause the system to produce zero photocurrent.

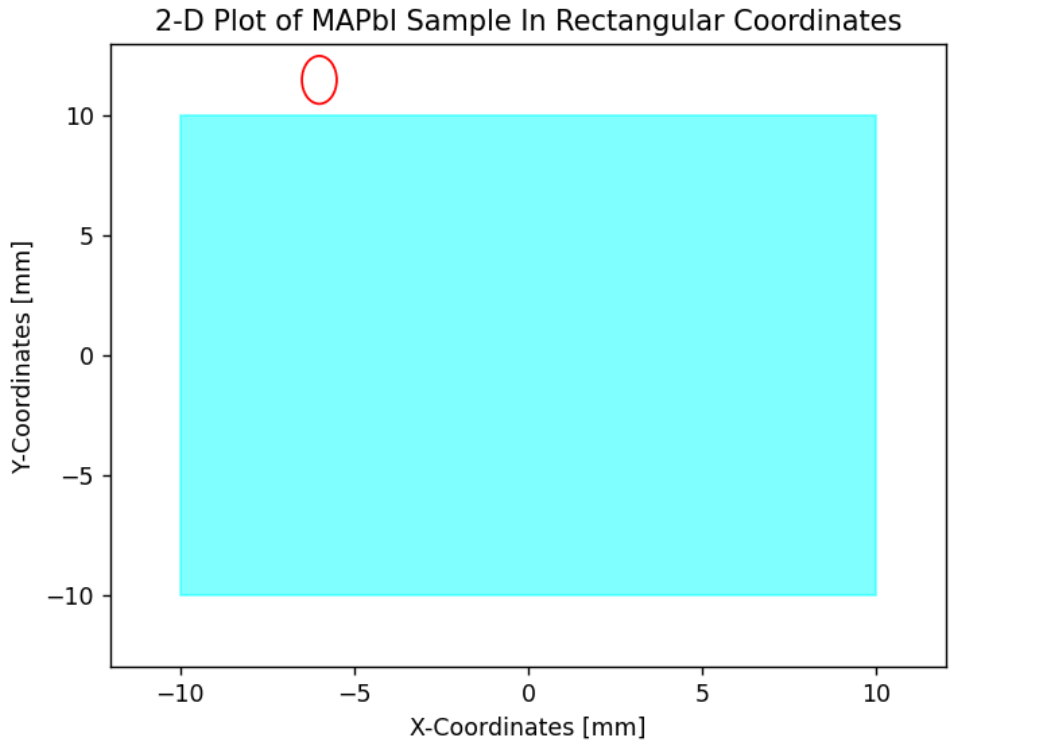

Figure 3.3: A depiction of a case where the x-ray beam produce a photocurrent

Additionally, another undesirable case would be one in which the beam does make contact with the surface of the film, but the beam does not make full contact with the film, shown in Figure 3.4.

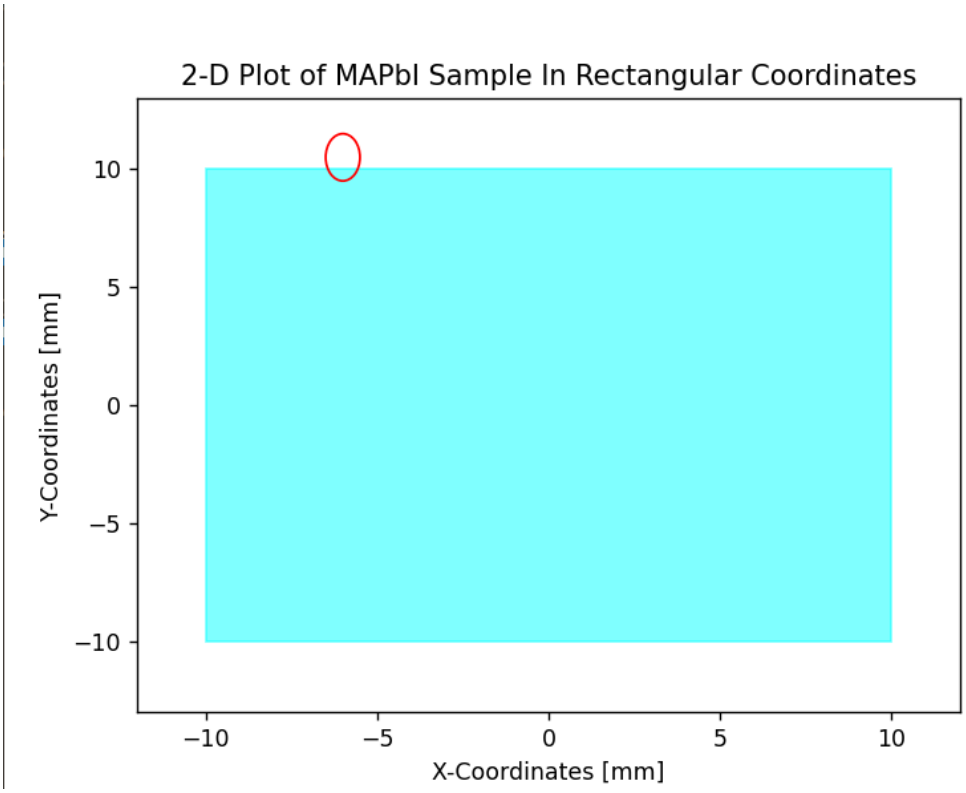

Figure 3.4: A depiction of a case where the x-ray beam produces a sub-optimal photocurrent

This would also not be ideal since the photocurrent produced would not be an accurate reflection of how well the material performs electronically. From the photoelectric effect, it follows that:

$$I_{\varphi,obs} \propto \phi_{p,s} \tag{3.1}$$

where $I_{\varphi,obs}(t)$ is the observed generated photocurrent and $\phi_{p,s}(t)$ is the scalar flux of photons which successfully interact with the photoelectron-producing sample. Since the focused x-ray beam is a very small ellipse of major radius 1 millimeter and minor radius 0.5 milimeters [6], The beam's spot will have to be adjusted along the relative x-y plane in small increments to confirm its relative position on the film itself. As it is incrementally moved along the x or y position the photocurrent produced will have to be monitored to see when the trend in photocurrent production rises, falls and plateaus. Once on the film, the beam spot will reach a peak photocurrent value, and additional movements along either the x or y axis will have negligible effect until the beam reaches the other side of the chip. Then, as the beam spot moves further off the film, the observed photocurrent will then drop proportionally with the areal amount by which the beam spot goes off the film. Building on the basic relation established by Equation 3.1, we may then conclude:

$$\frac{I_{\varphi,obs}(x,y)}{\max(I_{\varphi,obs})} = \frac{\int_a^b f_e(y)dy}{A_{e,tot}} \tag{3.2}$$

where $\int_a^b f_e(y)dy$ is the integral of the function of y describing the portion of the ellipse on the methylammonium lead iodide film and $A_{e,tot}$ is the total area of the ellipse characterizing the spot

of the beam generated by the x-ray source.

To demonstrate the implications of this equality, and to show what a sample data set from a run of this experiment may look like, a simple Python script was implemented. Shown in Figure 3.5 was a plot of the path of travel for a run where the beam traverses the full y-axis length of the film.

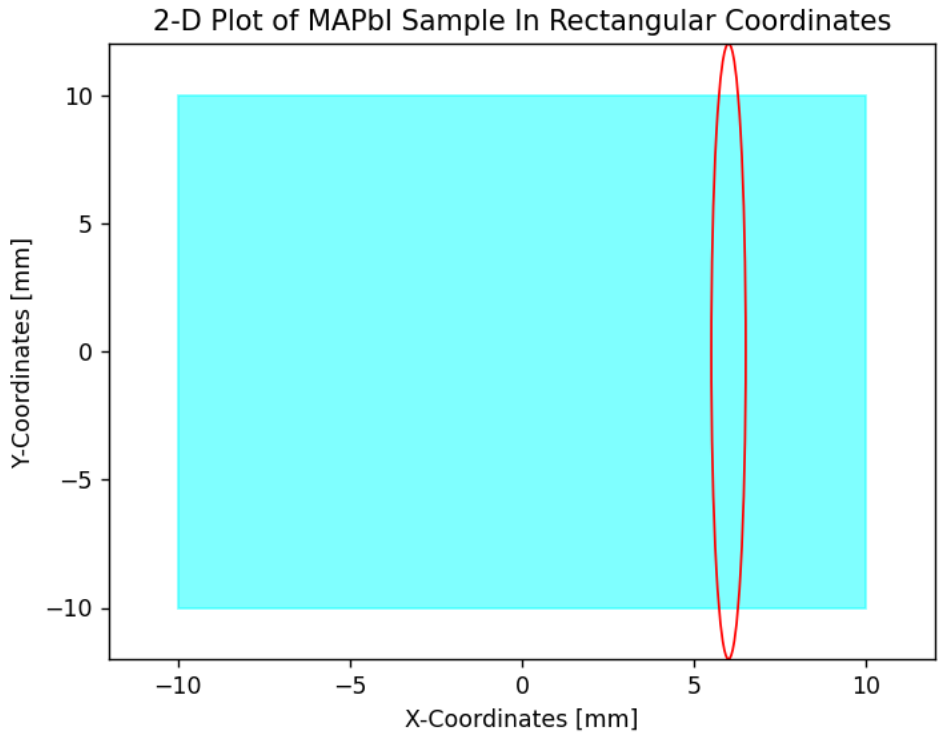

Figure 3.5: An outline of the path of travel for a run of the x-ray beam along the y axis

The predicted ratio of induced photocurrent to the expected maximum values was then plotted as a function of position. This trend may be observed in Figure 3.6.

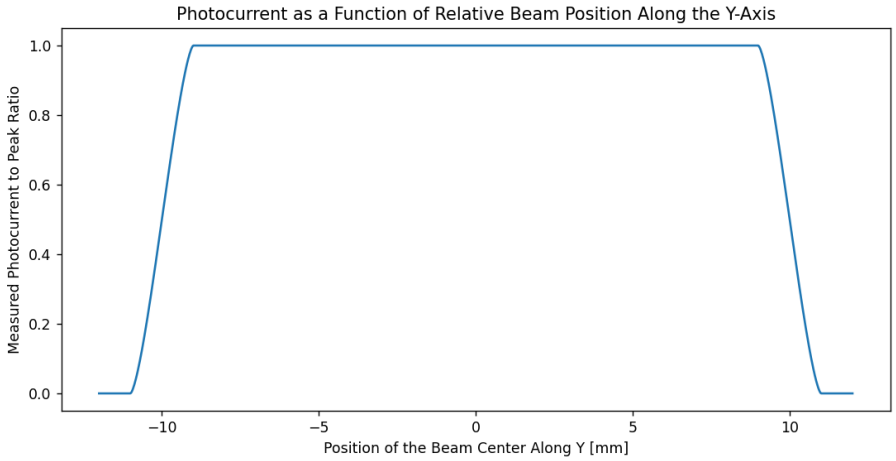

Figure 3.6: A plot of the ratio of observed to peak induced photocurrent as a function of the beam center's position along the y-axis

The full Python script used to generate this graph may be found in Appendix C.

Chapter 4

Discussion of Results

4.1 Discussion of Results

Beginning with the calculations from IMD, relevant optical measurements were then made for a fixed angle across a range of photon energies of interest.

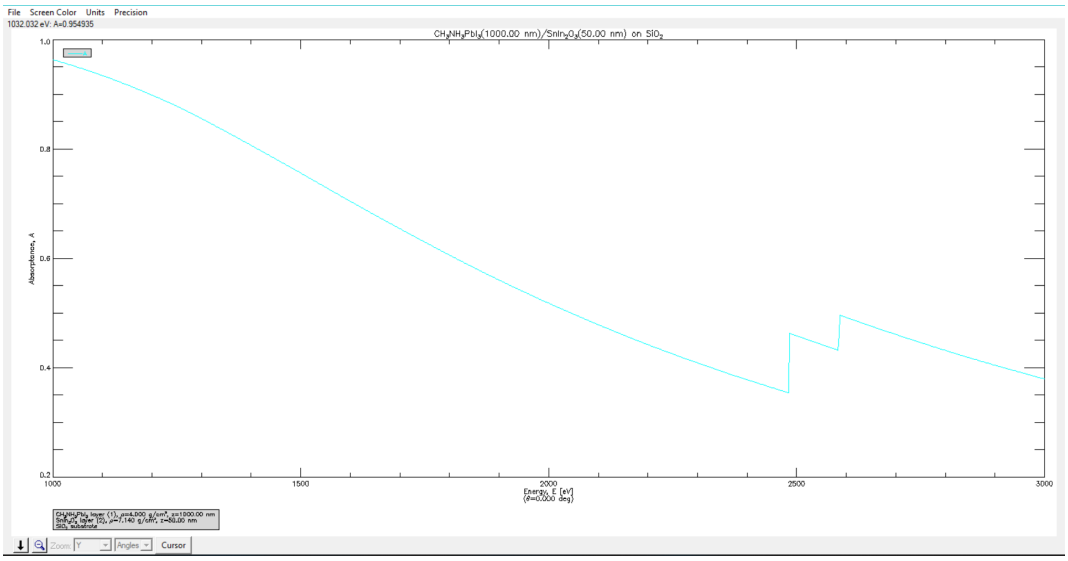

Figure 4.1: Plot of IMD generated results for absorption as a function of photon energy assuming orthogonal angle of incidence

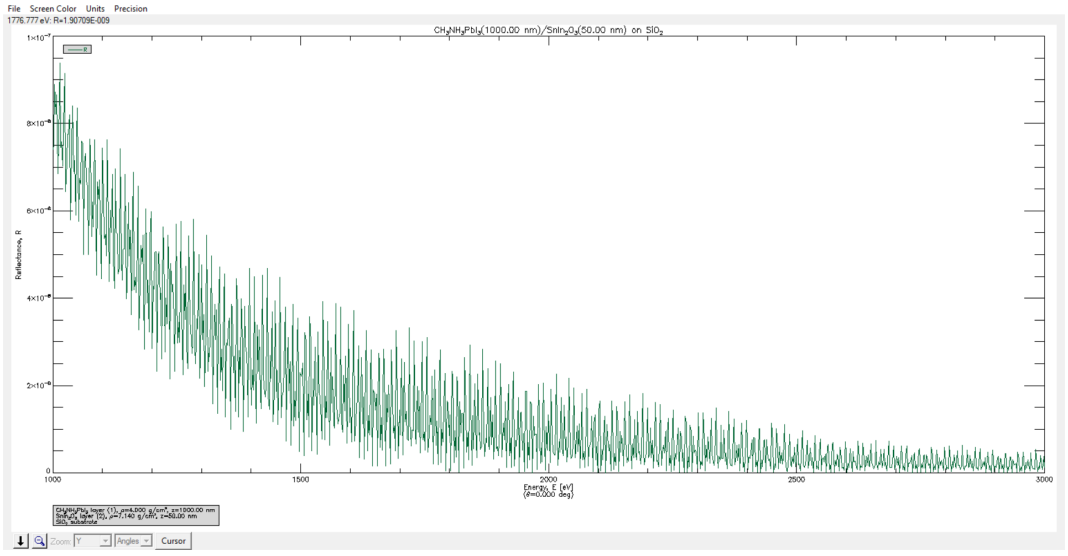

Figure 4.2: Plot of IMD generated results for reflection as a function of photon energy assuming orthogonal angle of incidence

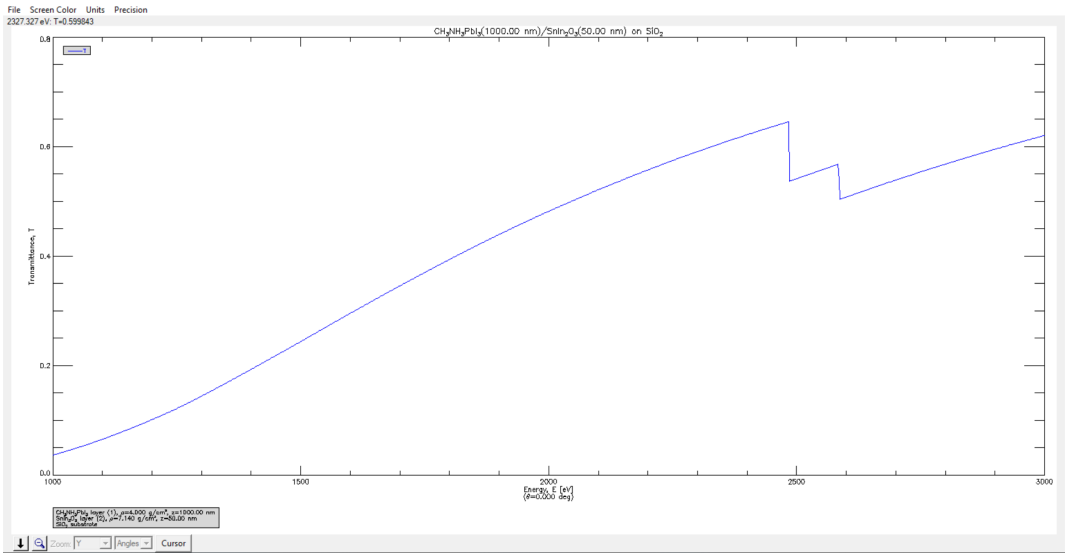

Figure 4.3: IMD main screen with cross-sectional sample display

The same parameters were calculated across a range of angles of incidence from a perpendicular incidence to parallel. Since the energy span calculations showed that as photon energy increases, the likelihood of interaction with the target generally decreases, which is typical of optics experiments dealing with photons of relatively high energy. For this reason, angular dependence calculations were made with a fixed incident photon energy of the lower energy bound of interest, 1 keV.

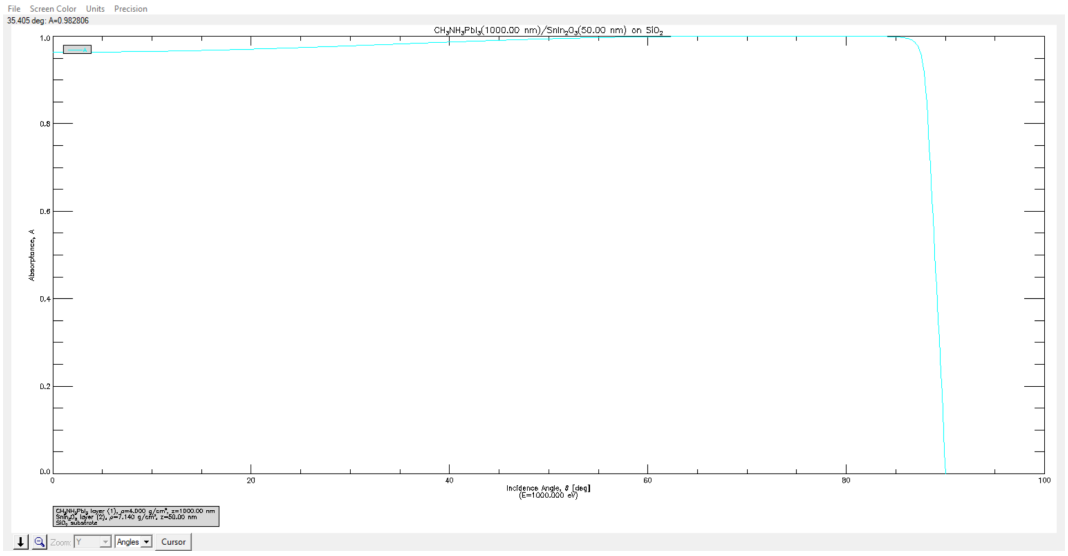

Figure 4.4: Plot of IMD generated results for absorption as a function of incidence angle for a fixed incident photon energy of 1 keV

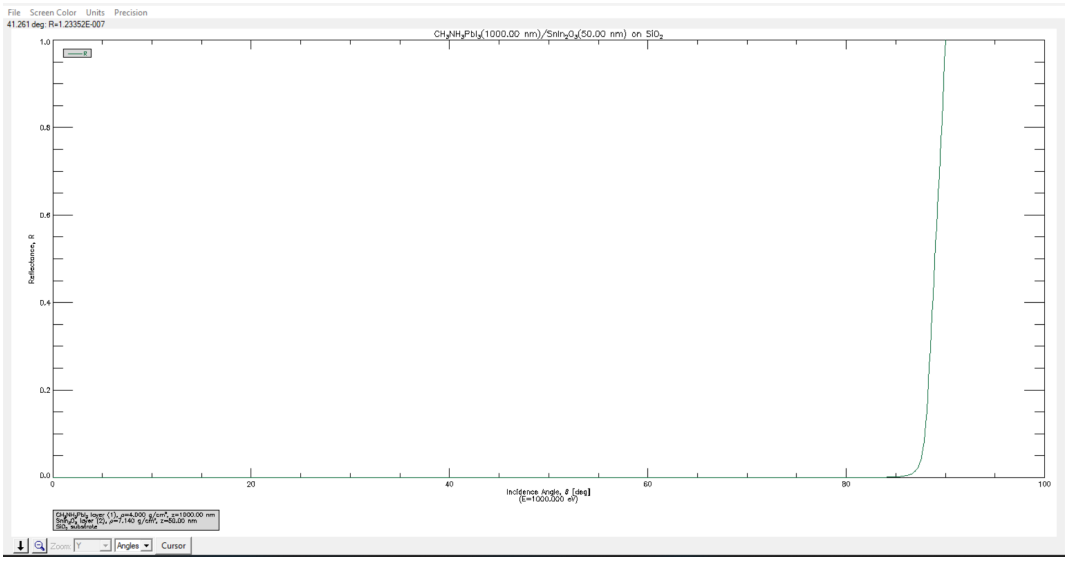

Figure 4.5: Plot of IMD generated results for reflection as a function of incidence angle for a fixed incident photon energy of 1 keV

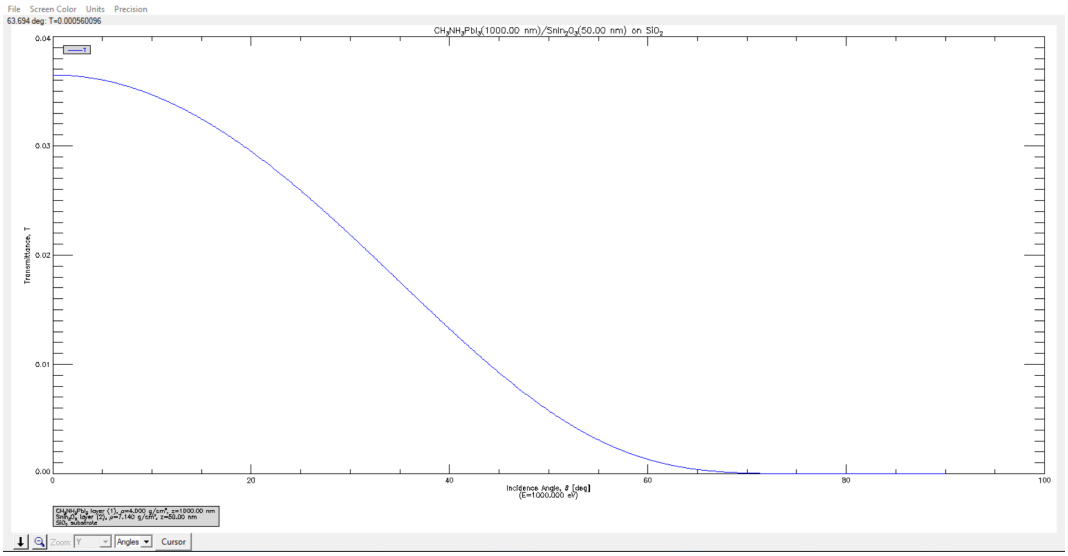

Figure 4.6: Plot of IMD generated results for transmittance as a function of incidence angle for a fixed incident photon energy of 1 keV

A final combined plot of all the values computed was also produced, which can be seen in Figure 4.7. Here, the angles of incidence calculated for ranged from 0 degrees to 180 degrees. By the programming of IMD, this was equivalent to a range of incidence angles ranging from perpendicular with respect to the sample entering on the vacuum side of the sample, to perpendicular with respect to the sample entering on the substrate side of the sample.

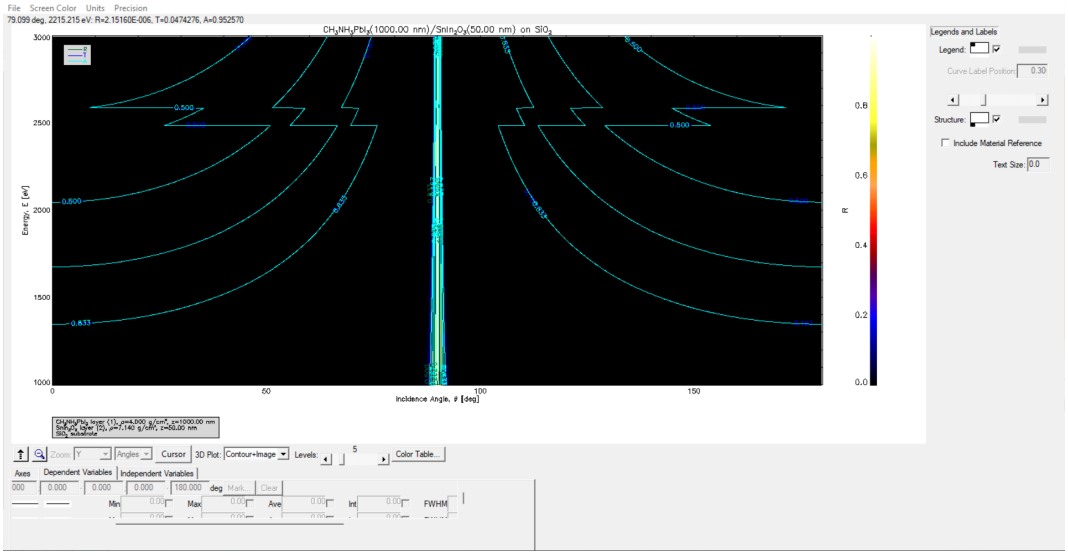

Figure 4.7: IMD calculated contour plot detailing Absorption, Transmittance, and Reflection as functions of incident photon energy and angle of incidence

Results from these calculations supported the hypothesis that the selected substrate would have negligible impact on the sample's overall optical properties. Beyond direct comparison numerical results, this is also evident from the strong symmetry of the graph about $\theta = 90$ degrees. For clearer inspection, the same plot concentrated around these angles is shown in Figure 4.8.

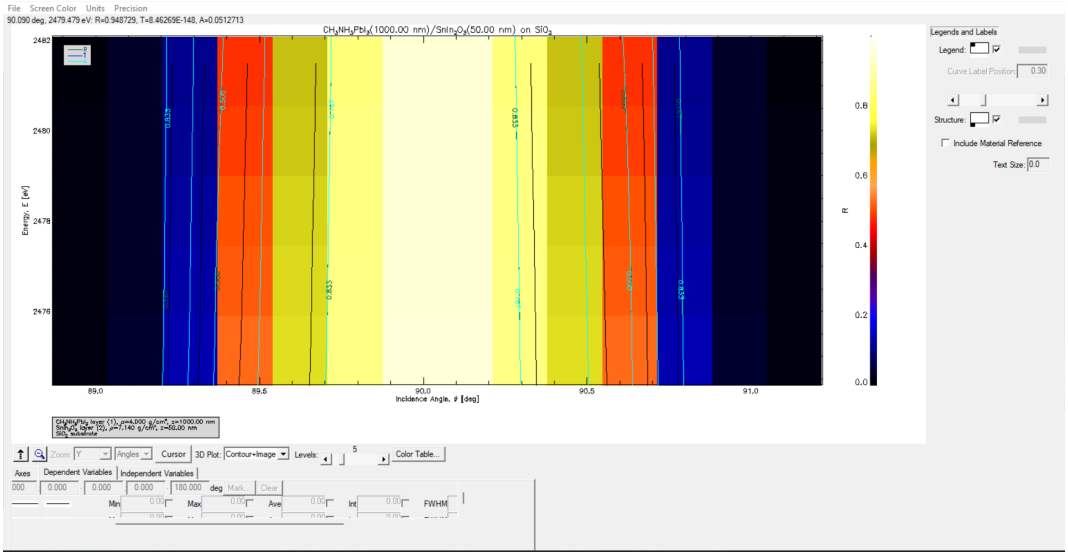

Figure 4.8: IMD calculated contour plot with increased zoom at near-horizontal angles

Due to the strong response of the incoming photons only at near-parallel angles of incidence, this produces the discontinuity observed between 85 and 95 degrees. This is not a property unique to any of the materials in the sample, but rather a consequence of physically thin films.

Overall, IMD shows that even for a very thin film of the material, the sample is capable of maintaining a strong absorption coefficient even at higher photon energies. The calculations from

IMD have also shown that this sample exhibits very little reflection and transmission of soft x-rays, even for an idealized model of the film with no surface roughness. A thicker model with increased surface roughness would likely further enhance the film's photon absorbing capabilities.

After the run in IMD showed a significant amount of absorption in the film sample, the other model sample was then run in MCNP6.2. Results from the tally for the aluminum anode run showed an average energy deposition of approximately 4.6E-04 MeV/g, while results from the tally for the silver anode run showed an average photon energy deposition of approximately 2.65E-04 MeV/g compared to the incident photon energies of 1.48E-3 MeV and 2.984E-3 MeV, respectively. In both cases, nearly all of the energy deposited was in the form of electron excitation. This means that of the photons captured in each simulation, a significant amount of energy was retained in the form of what would be photo-ionization in a real-world trial. As anticipated, the higher energy photon had deposited less energy in the sample overall, but still was able to capture at least 8% of the photon's energy. Both runs were simulated for 3E7 particle histories, passing all ten standard statistical checks MCNP automatically makes with each run, and had a final relative tally error of less than 2% in each case.

Chapter 5

Conclusions

5.1 Summary of Results and Comparison to Objectives

In this project, the results of computation were interpreted to make a determination as to if this material could be useful for plasma system diagnostics, and, if so, to what degree. Based on these results, several scenarios were predicted. One anticipated outcome was that there would be a possible current production of less than 1 microampere, but greater than 1 picoampere. This would mean that with the help of other standard detector electronics, a novel detector technology may be possible. Another possible outcome of the experiment is, if observed photocurrents are sufficiently large, in excess of 1 micro-Ampere, a possible method of energy recapture that would convert what would otherwise be lost energy from the system directly into usable electrical energy. Conversely, if hard-to-detect, weak photocurrents undetectable to even a picoammeter were detected, then the results of this project would serve as a rigorous counter-proof that such material is not viable to be used in electronic diagnostic systems within a nuclear fusion device. Considering the percentage of x-ray photons captured in the IMD and MCNP simulations, and the amount of energy captured from those the x-rays, methylammonium lead iodide has potential to produce sufficient photocurrent as a new radiation detector. However, considering that beyond 2.5 keV of photon energy, the absorption probability and energy collected overall energy from those photons declines by over 20% in absorption, and by almost 50% in total energy deposition, the material will likely not be a practical energy recapture mechanism in fusion devices.

5.2 Future Work

Though preliminary work from this project has lead to promising results, there are certainly plenty of areas in which further developments could be made in order to determine if this material is truly usable for supplying detection signals in a fusion device. The most obvious aspect of this project to expand on would be to confirm the computational results yielded by running the experiment as proposed in the real-world. The computations made in this project relied on several key assumptions, which would not necessarily be true in the real world. Another significant area of further development would be testing the material in a neutron field. If the sample described in this project were coated with a material that has a high interaction rate with neutrons, but is essentially invisible to x-rays, this could potentially allow it to be functional in an actual fusion device. Another important determining factor for whether this material would be qualified for used in a fusion device is its ability to withstand bombardment from leakage neutrons. The methodologies laid out in this report may also serve to guide future experimenters seeking to accomplish similar outcomes in the future with alternative materials.

Bibliography

[1] Walter Guttenfelder and Filippo Scotti. *NSTX-U render*. Princeton University, 2022.

[2] Takashi Okazaki. *Operation Control and Diagnostic Systems*, chapter 18, pages 501–537. John Wiley & Sons, Ltd, 2022.

[3] Nie Luo, Magdi Ragheb, and George H. Miley. Proton bremsstrahlung and its radiation effects in fusion reactors. *Fusion Engineering and Design*, 85(1):39–45, 2010.

[4] R. J. Goldston and P.H. Rutherford. *Introduction to Plasma Physics*. Introduction to Plasma Physics. Institute of Physics Pub., 1995.

[5] P. W. Chrisman, J. Clarke, and J. A. Rome. Magnetic island formation in a tokamak plasma from helical perturbations of the plasma current. In *(ORNL–TM–4501)*. Oak Ridge National Laboratory, 1974.

[6] user manual: monochromatic x-ray source rmc50 with options, May 2006.

[7] Minhuan Wang, Yulin Feng, Jiming Bian, Hongzhu Liu, and Yantao Shi. A comparative study of one-step and two-step approaches for mapbi3 perovskite layer and its influence on the performance of mesoscopic perovskite solar cell. *Chemical Physics Letters*, 692:44–49, 2018.

[8] Bandar Ali Al-Asbahi, Saif M.H. Qaid, Mahmoud Hezam, Idriss Bedja, Hamid M. Ghaithan, and Abdullah S. Aldwayyan. Effect of deposition method on the structural and optical properties of ch3nh3pbi3 perovskite thin films. *Optical Materials*, 103:109836, 2020.

[9] Bálint Náfrádi, Gábor Náfrádi, László Forró, and Endre Horváth. Methylammonium lead iodide for efficient x-ray energy conversion. *The Journal of Physical Chemistry C*, 119(45):25204–25208, 2015.

[10] Ito coated glass, Mar 2023.

[11] David L. Windt. Imd software for modeling the optical properties of multilayer films. *Computers in Physics*, 12(4):360–370, 1998.

[12] H. Wei and Huang J. Halide lead perovskites for ionizing radiation detection. *Nature*, March 2019.

Appendix A

MCNP Input Deck for Aluminum Anode Run

```
    MAPbI Film Irradiation, 1486.6 eV case
c Coleman Smith
c --- beginnning of cell cards for vessel ---
1 0        1 -2 -3 4 5 -6     $ Column of vacuum
2 1 -4.000 1 -2 -3 4 6 -7     $ Layer of MAPbI (CH3NH3PbI3)
3 2 -7.140 1 -2 -3 4 7 -8     $ Column of SnIn2O3 (ITO coating)
4 3 -2.650 1 -2 -3 4 8 -9     $ Column of SiO2 (Glass)
5 0        #1 #1 #3 #4 -10    $ Bounding sphere
6 0        10                 $ Outside universe
c *** end of cell cards for sample problem ***

c --- beginning of surfaces for vessel ---
1 PZ 0             $ Lower bound for slabs
2 PZ 2             $ Upper bound for slabs
3 PY 1             $ Left bound for slabs
4 PY -1            $ Right bound for slabs
5 PX 0             $ Back bound for slabs
6 PX 1             $ Void outer bound
7 PX 1.0001        $ CH3NH3PbI outer bound
8 PX 1.000119      $ SnIrO outer bound
9 PX 1.100119      $ SiO outer bound
10 SO 2000         $ Bounding sphere
c *** end of surfaces for vessel ***

c --- beginning of material cards ---
m1 $ CH3NH3PbI3, 4.0 g/cc
      6000    0.083333    $  C
      1000    0.500000    $  H
      7000    0.083333    $  N
     82000    0.083334   $  Pb
     53000    0.250000   $  I
m2 $ Sn:In2O3, 7.41 g/cc
     50000    0.166666   $  Sn
     49000    0.333334   $  In
```

```
      8000    0.500000   $  O
m3 $ SiO2, 2.65g/cc
     14000    0.333334   $ Si
      8000    0.666666   $ O
c *** end of material cards ***
c
c --- beginning of data cards ---
c + beginning of source definition ---
c + rectangular plane source centered on the origin and perpendicular
c to the y-axis. This uses a degenerate Cartesian volumetric source.
c
SDEF POS=-1 0 0 DIR = 1 VEC= 1 0 0 X=0 Y=d1 Z=d2 PAR=2 ERG=0.0014866
SI1 -50 50 $ sampling range Ymin to Ymax
SP1 0 1    $ weighting for y sampling: here constant
SI2 0 100  $ sampling range Zmin to Zmax
SP2 0 1    $ weighting for z sampling: here constant
F6:P 2     $ Energy dep. in CH3NH3PbI3 layer
mode p
imp:p 1 1 1 1 1 0
nps 3e7
c *** end of data cards ***
c
PRINT
```

Appendix B

MCNP Input Deck for Silver Anode Run

```
MAPbI Film Irradiation, 2984.3 eV case
c Coleman Smith
c --- beginnning of cell cards for vessel ---
1 0        1 -2 -3 4 5 -6     $ Column of vacuum
2 1 -4.000 1 -2 -3 4 6 -7     $ Layer of MAPbI (CH3NH3PbI3)
3 2 -7.140 1 -2 -3 4 7 -8     $ Column of SnIn2O3 (ITO coating)
4 3 -2.650 1 -2 -3 4 8 -9     $ Column of SiO2 (Glass)
5 0        #1 #1 #3 #4 -10    $ Bounding sphere
6 0        10                 $ Outside universe
c *** end of cell cards for sample problem ***

c --- beginning of surfaces for vessel ---
1 PZ 0             $ Lower bound for slabs
2 PZ 2             $ Upper bound for slabs
3 PY 1             $ Left bound for slabs
4 PY -1            $ Right bound for slabs
5 PX 0             $ Back bound for slabs
6 PX 1             $ Void outer bound
7 PX 1.0001        $ CH3NH3PbI outer bound
8 PX 1.000119      $ SnIrO outer bound
9 PX 1.100119      $ SiO outer bound
10 SO 2000         $ Bounding sphere
c *** end of surfaces for vessel ***

c --- beginning of material cards ---
m1 $ CH3NH3PbI3, 4.0 g/cc
      6000    0.083333    $  C
      1000    0.500000    $  H
      7000    0.083333    $  N
     82000    0.083334    $  Pb
     53000    0.250000    $  I
m2 $ Sn:In2O3, 7.41 g/cc
     50000    0.166666   $  Sn
     49000    0.333334   $  In
```

```
      8000    0.500000   $  O
m3 $ SiO2, 2.65g/cc
     14000    0.333334   $ Si
      8000    0.666666   $ O
c *** end of material cards ***
c
c --- beginning of data cards ---
c + beginning of source definition ---
c + rectangular plane source centered on the origin and perpendicular
c to the y-axis. This uses a degenerate Cartesian volumetric source.
c
SDEF POS=-1 0 0 DIR = 1 VEC= 1 0 0 X=0 Y=d1 Z=d2 PAR=2 ERG=0.0029843
SI1 -50 50 $ sampling range Ymin to Ymax
SP1 0 1    $ weighting for y sampling: here constant
SI2 0 100  $ sampling range Zmin to Zmax
SP2 0 1    $ weighting for z sampling: here constant
F6:P 2     $ Energy dep. in CH3NH3PbI3 layer
mode p
imp:p 1 1 1 1 1 0
nps 3e7
c *** end of data cards ***
c
PRINT
```

Appendix C

Python Code Used for Beam Traverse Calculation

```
# SHC Thesis Circ In Squ
# Created by Coleman Smith on 03/24/23
# Built for SP23 Schreyer Honors Thesis

from matplotlib.patches import Ellipse
from matplotlib.patches import Rectangle
import matplotlib.pyplot as plt
import numpy as np
import math

# Get user input for square and ellipse starting coordinates (
    fixed chip and beam dimensions)
square_x = 0
square_y = 0
square_size = 20
ellipse_width = 1
ellipse_height = 2
ellipse_x = float(input("Enter the x-coordinate of the beam
    ellipse's center (mm): "))
ellipse_y = float(input("Enter the y-coordinate of the beam
    ellipse's center (mm): "))

# Create a new figure
fig, ax = plt.subplots()

# Draw the square
square = Rectangle((square_x - square_size / 2, square_y -
    square_size / 2), ...
square_size, square_size, fill=True, edgecolor='cyan', facecolor
    ='cyan', alpha=0.5)
ax.add_patch(square)

# Draw the ellipse
```

```
ellipse = Ellipse((ellipse_x, ellipse_y), ellipse_width,
   ellipse_height, fill=False, edgecolor='red')
ax.add_patch(ellipse)

# Set the axis limits based on the size of the square
ax.set_xlim(square_x - square_size / 2 - 1 - ellipse_width,
   square_x + square_size / 2 + 1 + ellipse_width)
ax.set_ylim(square_y - square_size / 2 - 1 - ellipse_height,
   ellipse_y + ellipse_height + 1)

# Label Axes and Make Title
plt.title('2-D Plot of MAPbI Sample In Rectangular Coordinates')
plt.xlabel('X-Coordinates [mm]')
plt.ylabel('Y-Coordinates [mm]')

# Ask for # of trials to simulate
n_trials = int(input("Enter the desired number of simulated
   trials: "))

# Find A_tot
A_tot = np.pi*ellipse_height*ellipse_width/4
print(A_tot)

# Perform A_spot/A_tot calculation for a positive-y-starting beam
# traverse accross the film (first half of data set)
d_axis = np.linspace(-ellipse_y,ellipse_y,2*n_trials)
I_xy_I_0 = []
y_start = ellipse_y
increment = ellipse_y/n_trials
for i in range(0,n_trials):
    if y_start - ellipse_height/2 > square_size/2:
        I_here = 0
    elif y_start + ellipse_height/2 <= square_size/2 :
        I_here = 1
    elif y_start < ellipse_height/2 + square_size/2 and y_start >
        square_size/2:
        x_here = y_start - square_size/2
        print(x_here)
        I_here = A_tot/2 - (0.5*x_here*math.sqrt(1-x_here**2)
           +0.5*np.arcsin(x_here))
        I_here=I_here/A_tot
    elif y_start <= square_size/2 and y_start > square_size/2 -
       ellipse_height/2:
        x_here = square_size/2 - y_start
        print(x_here)
```

```
            I_here = A_tot/2 + (0.5*x_here*math.sqrt(1-x_here**2)
                +0.5*np.arcsin(x_here))
            I_here=I_here/A_tot
        else:
            I_here = 0
        I_xy_I_0.append(I_here)
        y_start-=increment
print(I_xy_I_0)

# Mirror first half of data due to problem symmetry
other_half = np.flip(I_xy_I_0)
print(other_half)
i=0
while i<len(other_half):
    I_xy_I_0.append(other_half[i])
    i+=1

# Plot simulated results
plt.figure()
plt.plot(d_axis,I_xy_I_0)

# Configure Axes and Labels
plt.title('Photocurrent as a Function of Relative Beam Position
   Along the Y-Axis')
plt.xlabel('Position of the Beam Center Along Y [mm]')
plt.ylabel('Measured Photocurrent to Peak Ratio')

# Show the plots
plt.show()
```

Academic Vita

Coleman P. Smith

Education

Bachelor of Science in Nuclear Engineering
Schreyer Honors College at The Pennsylvania State University,
University Park, PA (Expected) Spring 2023

Personal Summary

A self-motivated nuclear engineer who is passionate about breakthroughs and innovation in nuclear science. Strong interest in uniting the theoretical with the experimental as well as the development of new technological solutions to improve the efficiency of the nuclear industry.

Professional and Research Experience

Undergraduate Research Assistant Radiation Science and Engineering Center, The Pennsylvania State University, University Park, PA; Dec. 2021 - Dec. 2022

- Gained experience in modeling of fluid flow cases for reactor components and microfluidic chips for radioisotope solvent exchange.
- Worked with CFD software such as Nek5000 and Ansys Student to compute fluid mechanics solutions

Senior Reactor Operator, Radiation Science and Engineering Center, The Pennsylvania State University, University Park, PA; Jan. 2019 – Present

- Developed fluency in Python and C++ programming languages while designing and implementing control software for neutron transmission system.
- Gained experience in using Monte-Carlo software such as MCNP to model radiation from various sources

Publications

Smith, Coleman P. and Bistany, Sean P., "Feasibility of High-Frequency Radiation for Electrical Energy Generation" American Nuclear Society Student Conference 2022 Technical Track Papers, March 2022

Presentations

"Feasibility of High-Frequency Radiation for Electrical Energy Generation." Paper Presented at *The American Nuclear Society Student Conference*, Urbana, IL. April 15, 2022

Professional Associations

- American Nuclear Society (ANS)
- Alpha Nu Sigma National Honor Society ($AN\Sigma NHS$)
- Institute of Nuclear Materials Management ($INMM$)
- Women in Nuclear (WIN)

Related Coursework and Skills

- Java, C++, MATLAB, HTML, and Python programming languages;
- LabView;
- SolidWorks, SketchUp;
- MCNP, OpenMC;
- Nek5000, Ansys Fluent